Essentially, all models are wrong, but some are useful

George E.P. Box,

(Box and Draper, 1987)

5

Advanced fracture models

5 ADVANCED FRACTURE MODELS

In the previous chapter it was shown that the MOR parameter cannot be relied upon to predict the peak load and post crack behaviour of different sized structural elements in flexure. In this chapter, the aim is to devise a fracture mechanics damage model for the material. The damage function will be based on the specific fracture energy (G_f) and tensile strength (f_t) parameters determined for the high performance fibre reinforced concrete in the previous chapter. The hypothesis is that such a model would allow better prediction of the flexural capacity of the material. A further purpose of the numerical modelling is to validate the methodology used to determine the fracture parameters as presented in the previous chapter.

The second aim of this chapter is to test the hypothesis that the accuracy, and possibly the precision, of fatigue prediction models for the material can be improved through the use of fracture mechanics concepts. The findings of the monotonic and cyclic loading experiments are combined in order to devise a model for the prediction of fatigue in UTCRCP material.

The development and validation of the fracture mechanics damage models for the material are discussed in Section 5.1. The work in Section 5.2 demonstrates that the numerical models allow the numerical simulation of fracture in beam and centrally loaded disk specimens. The models can be used to predict size effect observed in the experiments. In Section 5.3 the numerical models are adjusted to allow the simulation of flexural behaviour of beams containing rebar. The results of the numerical simulation of the cylinder splitting tests are presented in Section 5.4. In Section 5.5 the numerical models developed in the study are used to simulate fracture in examples of full size pavement structures. Models for the prediction of fatigue using conventional methods and fracture mechanics based approaches are developed

in Section 5.6. The final section of this chapter contains a discussion on the numerical fracture models put forward by this study.

5.1 Development of fracture models

According to the cohesive softening model, the material behaves linear elastically until the principal stress reaches the tensile strength of the material, at which point a crack is induced. The linear elastic part of the material response in the numerical simulation is defined by the values for Young's modulus and Poisson's ratio in Table 4-1. For the post cracking behaviour of the material a suitable mathematical softening functions had to be developed. Several different types of post crack cohesive softening functions used for fibre concrete were discussed in Section 2.5. Initially, a simple exponential shape was used for the softening function. Later in the study, the exponential model was replaced by more advanced softening function with crack tip singularity.

A damage function for failure in compression was not included as part of the study. The compressive stresses in the numerical simulation of the flexural tests were monitored to ensure that the compressive stress did not significantly exceed the compressive strength.

5.1.1 Development of exponential tensile softening function

The exponential softening function was developed after completion of the first round of testing. The main advantage of the exponential softening function is that only the tensile strength of the material and the fracture energy need to be known to fully define the shape. Other approaches invariably require tests performed on samples with a range of sizes and a constant geometry, and/or measurement of the crack mouth opening displacement, and/or the use of loading-unloading procedures during the test. This type of detailed information on the post crack behaviour was not available at this early stage of the study. Exponential softening was considered a suitable starting point for the analysis due to the fact that the post crack behaviour of fibre reinforced concrete shows a steep initial drop off in stress followed by a long tail of gradual softening.

The exponential softening functions developed as part of this study for the first four mixes tested, are shown in Figure 5-1. In the numerical simulation, elements respond linear

elastically until the set tensile strength for the material is exceeded, at which point a cohesive crack is formed in the element. After induction of the crack, stress (σ) is transferred across the crack faces following the exponential function of the crack width (w):

$$\sigma = \mathrm{f}(w) = f_t \mathrm{e}^{\frac{-wf_t}{G_f}} \qquad (5.1)$$

The stress transferred over the crack reduces exponentially towards zero with the increase of the crack width. This is an acceptable approximation, as in reality the critical crack width for the total softening function is very large. A situation of zero stress transfer will only be reached when the crack width is equal to half the length of the steel fibres (i.e. ½ x 30 mm) and all fibres in a unit area have been pulled out completely.

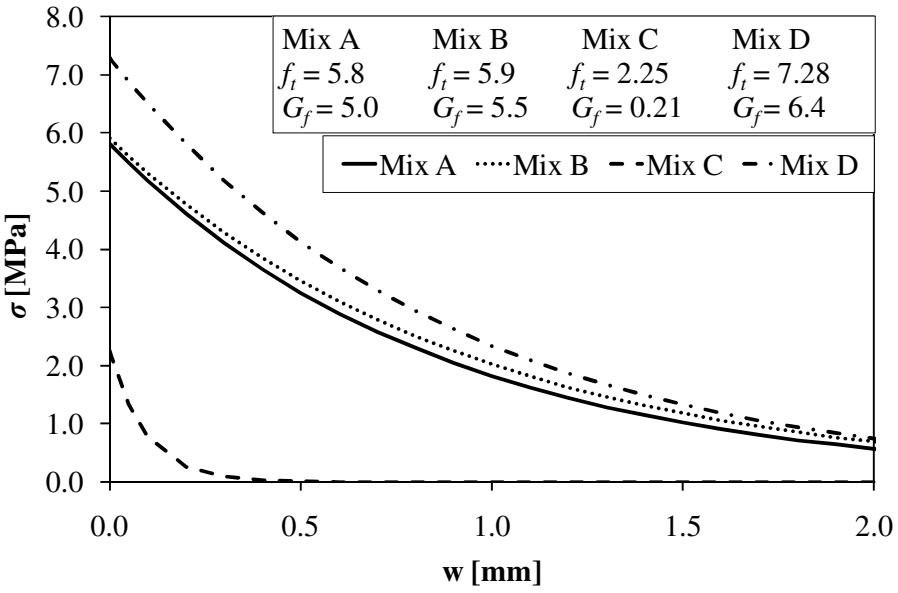

Figure 5-1: Exponential softening functions used for Mix A,B,C,D

The exponential softening function was used to simulate the flexural tests performed on Mix A, B, C and D beam specimens. It was found to be possible to obtain acceptable results from the numerical simulation using the exponential softening function. The results of the numerical simulation in OpenSees for the various specimen sizes are provided in Appendix C. Figure 5-2 shows the results of the numerical simulation with exponential softening for TPB1-A as an example. The figure shows the results for two simulation runs. One (f_t = 6.4)

was performed using the tensile strength obtained from the tensile splitting test, the other (f_t = 5.8) represents a best fit to data determined by means of a parameter study.

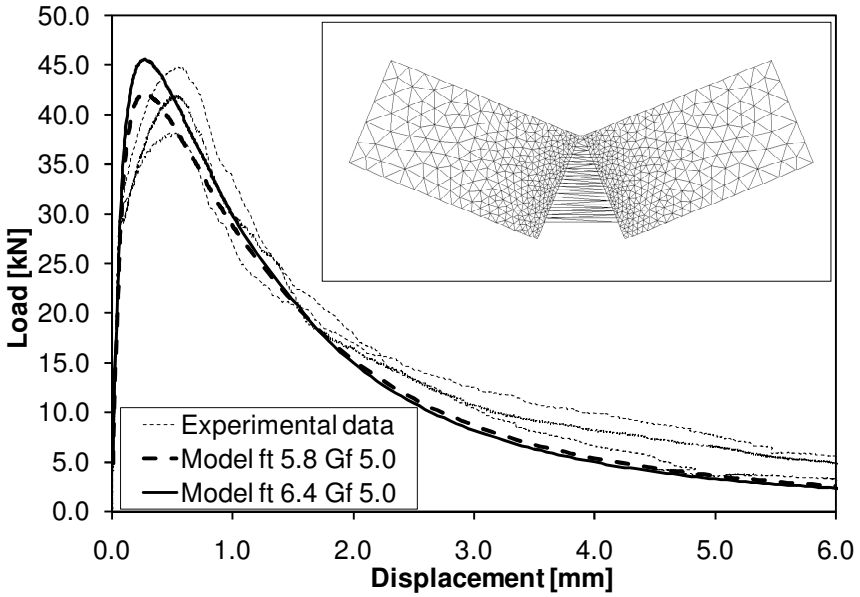

Figure 5-2: Numerical simulation of TPB1-A

With exception of the plain concrete, it was found that simulation using the exponential softening function and the value of f_t from the adjusted tensile splitting test as described in Section 4.4.3 with G_f as determined using the procedure in Section 4.4 leads to overestimation of the flexural capacity of the beams. In the early stages of this study it was not clear whether the error was due to the test method used to determine the fracture properties, or to the shape of the softening function. It was found that a good fit to data could be obtained for the fibre reinforced concrete flexural tests in both TPB and FPB configuration provided the tensile strength was calibrated. The optimized softening functions for the mixes A and B in Figure 5-1 therefore have reduced tensile strengths compared to experimentally determined values. The figures in Appendix C show the results for the numerical simulation using optimized softening functions. The simulation of Mix D tests was performed without calibration. In a publication on the size effect study performed on Mix D by Denneman et al. (2010a) it was simply noted that the exponential softening function leads to an overestimation of the flexural capacity when f_t is used uncalibrated. The simulation of the tests on the plain concrete Mix C specimens also reported in Denneman et al. (2010b) did not require

calibration as the simulation using the experimentally determined fracture properties allowed for acceptable results as shown in Figure 5-3.

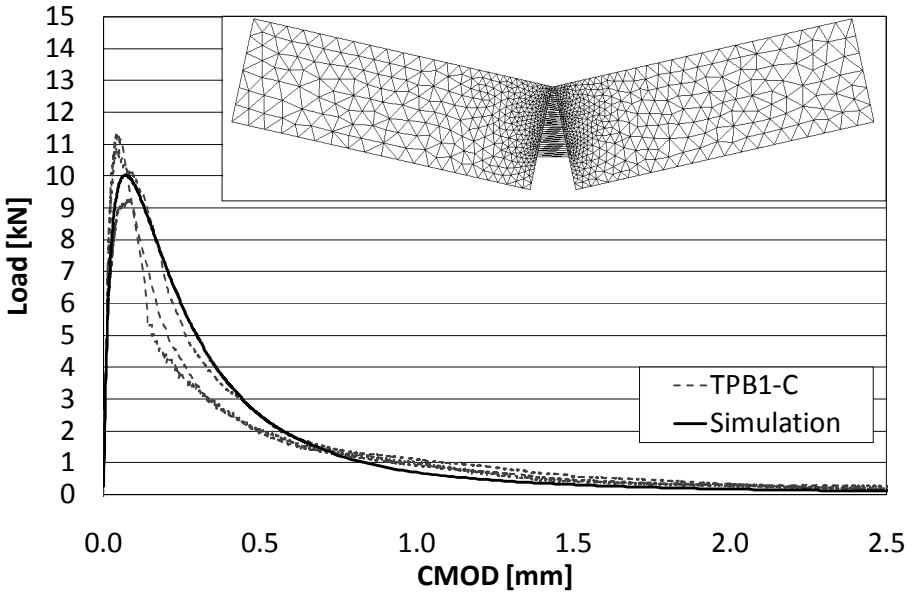

Figure 5-3: Numerical simulation of TPB experiments on plain concrete

Apart from the simulation of experiments performed as part of this study, the EDM with exponential softening function was also applied elsewhere. Wu et al. (2009) used it to model beam tests on asphalt and Denneman et al. (2009) applied it to fracture in concrete specimens. The model was further applied to simulate fracture in disk shaped direct tensile tests on asphalt as reported in Denneman (2010).

The exponential softening function allowed satisfactory simulation of the flexural beams, provided that the model was calibrated for the value of f_t. Through the modelling of the tensile splitting tests (discussed in Section 3.3.2), however it became clear that the simple exponential shape did not replicate the initial part of the softening behaviour of the fibre reinforced material well enough.

5.1.2 Improved exponential softening function with crack tip singularity

As described earlier in Section 2.5.7, Lim et al. (1987) studied the softening behaviour of concrete with a similar type of steel fibres from the same producer as used for this study. The study found that the material behaviour is best simulated using a softening function with an initial spike at high strength followed by a long tail at a lower stress. The rapid drop in stress at crack induction followed by more gradual degradation can be modelled using a crack tip singularity approach. Crack tip singularity is suitable for fibre reinforced composites, as it simulates the initial failure of the matrix followed by the slow pull out of the fibres (Bažant and Planas, 1997, Dupont and Vandewalle, 2004).

To improve on the fit of the numerical simulation allowed by the simple exponential softening function, a slightly more complex softening function with crack tip singularity followed by exponential softening was developed. The material behaviour in tension is shown schematically in Figure 5-4a. Initially the material behaves linear elastically until f_t, is reached. When the crack is introduced in the concrete, the stress drops until the fibres are activated. In the model it is assumed that the stress drops without an increase in crack width w, resulting in a crack tip singularity. The stress at the base of the singularity is the post singularity crack bridging stress (σ_1). After the initial drop in stress, the softening takes an exponential form.

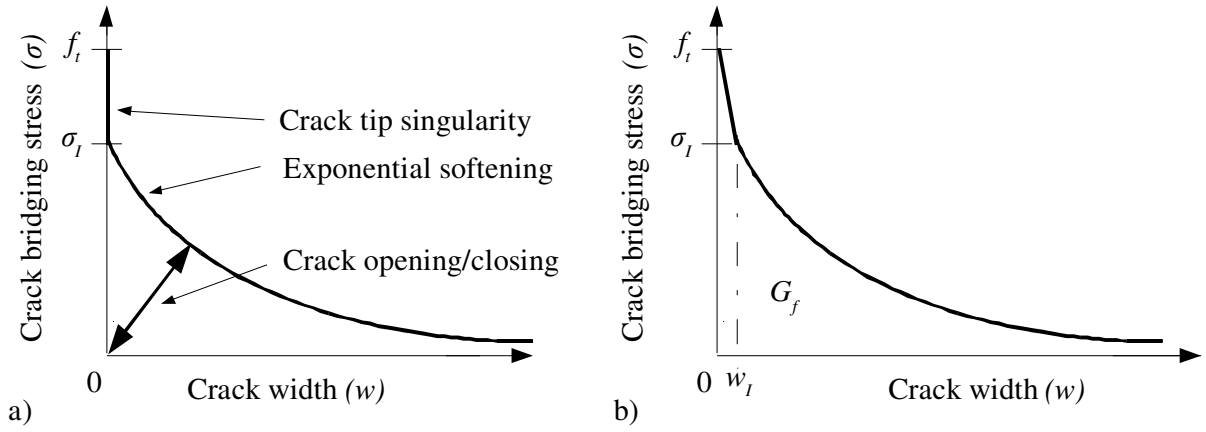

Figure 5-4a: Material behaviour in EDM simulation, b: Softening function as implemented in FEM as part of this study

To achieve the material behaviour shown in Figure 5-4a, a softening function combining a linear and an exponential part was implemented in the EDM code in OpenSees. The function is as shown in Figure 5-4b. When the tensile strength (f_t) of the material is reached a crack is formed, the stress transferred across the crack reduces linearly with an increase in crack width (w) for $0 < w < w_I$ according to:

$$\sigma = f_t\left(\frac{f_t - \sigma_I}{w_I}\right)w \tag{5.2}$$

Once w_1 is reached softening becomes exponential for $w_I < w < \infty$. The exponential softening is defined by value of σ_I and the remaining fracture energy $G_{f,I}$. This is the specific fracture energy G_f less the energy dissipated under the linear softening:

$$G_{f,I} = G_f - \left(\frac{f_t + \sigma_1}{2}\right)w_I \tag{5.3}$$

The exponential part of the softening function is given by:

$$\sigma = \sigma_I e^{(-a_I(w - w_I))} \tag{5.4}$$

With:

$$a_1 = \frac{\sigma_I}{G_{f,I}} \tag{5.5}$$

To create the softening curve with crack tip singularity shown in Figure 5-4a, w_I was initially set to 0 in the above equations for the simulation of flexural beam tests. As G_f is determined from the TPB results and f_t is obtained from tensile splitting tests, σ_I is the only unknown to be calibrated in the model. It was later found that if a small displacement w_I is allowed, a better fit of the model can be obtained for the tensile splitting tests. w_I was set to 0.005 mm, for reasons discussed in detail in Section 5.4. The final calibrated softening curves for the fibre reinforced mixes are shown in Figure 5-5. The curves were developed based on a parameter study to achieve the best fit for both the flexural beam and tensile splitting tests. The difference between the mixes in terms of post cracking stress capacity due to difference in mix composition and importantly fibre content is visible in Figure 5-5. The results of the numerical simulation using the crack tip singularity approach are shown in Appendix D.

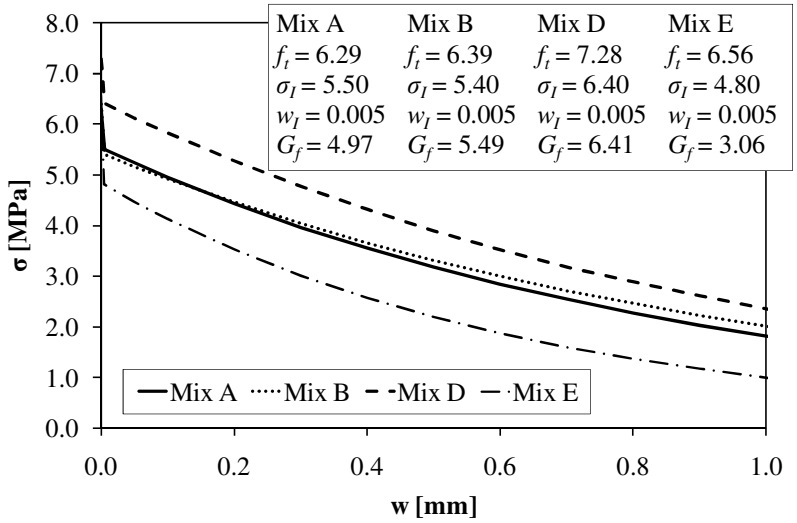

Figure 5-5: Optimized softening functions for studied mixes

5.1.3 Mesh size sensitivity

Researchers often opt for very fine meshes in and around the crack area to avoid issues with mesh size objectivity. In the EDM the crack is not restricted to follow element boundaries and nodal points and this relieves some of the mesh size requirements other FEM crack simulation approaches have. The primary consideration in choosing mesh size for the EDM used in this study is the prevention of crack locking. In the EDM the conditions for cracking and the direction of the crack are calculated at element level. As a result a discrete crack in the beam may lock when an element, typically at the crack tip, forms a crack in the direction perpendicular to the main crack direction. The EDM approach used for the present study includes a technique proposed by Sancho et al. (2007) to avoid crack locking on a local (element) level by allowing the direction of the crack to change and be solved for each analysis step while the crack width is small. Sancho et al. (2007) used crack width values in the range between 0.1-0.2 G_f/f_t as a threshold to fix the direction of the crack. For the present study a value of 0.2 G_f/f_t was applied with good results. Crack locking may still occur, and becomes more likely as the crack approaches the top of the beam. For successful calculations a balance needs to be found between the mesh size, the number of iterations per analysis step, and threshold width for the crack direction. As long as a reasonable number of elements are used in the fracture ligament area the model provides consistent results independent of mesh size. Figure 5-6 shows a comparison between the results of an analysis performed with a mesh size standard for this study (5 mm in the crack area) and an analysis with a very fine mesh (0.5 mm in the crack area). The resulting load-deflection curves are almost identical.

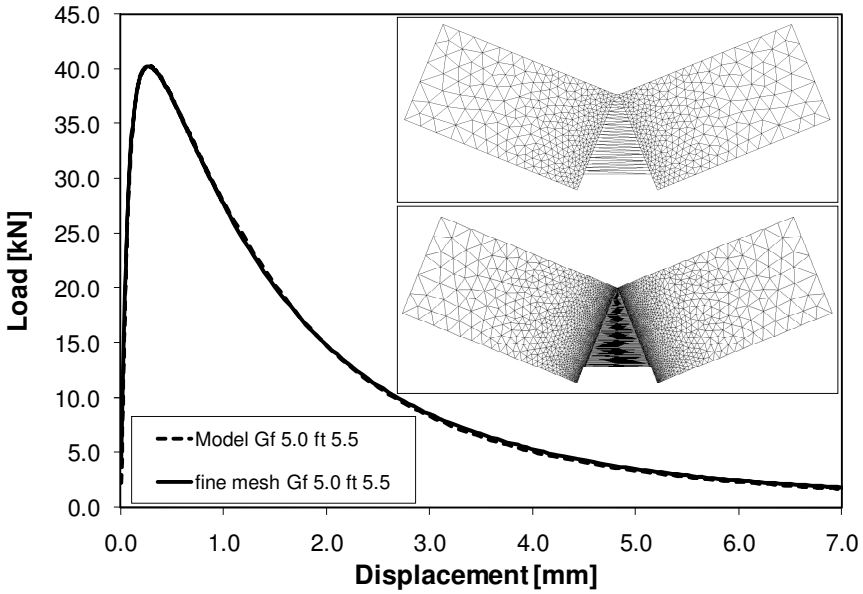

Figure 5-6: Comparison of EDM results using different mesh sizes.

5.1.4 Comparison of OpenSees and Abaqus models

To ensure that the fracture simulation using the Abaqus brittle cracking model with the softening functions developed in this study is equivalent to the results obtained from the EDM in Opensees, both approaches were applied to simulate a TPB test. The results of the numerical simulations of specimen type TPB1-A using the exponential softening function are shown in Figure 5-7.

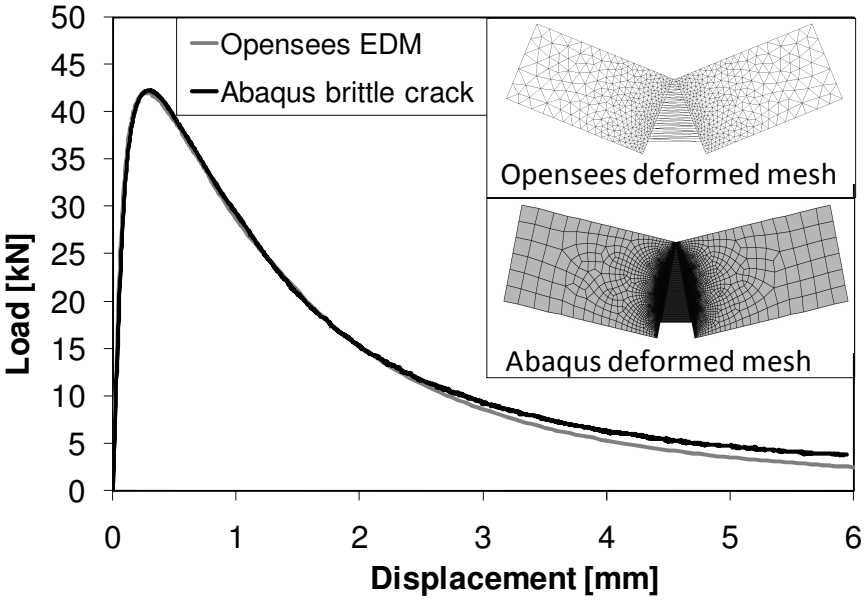

Figure 5-7: Comparison of numerical simulation using Opensees and Abaqus

A characteristic element size of 1 mm was used for both the triangular OpenSees elements and the Abaqus quadrilateral elements in the ligament area above the notch. At the far edges of the mesh, the characteristic size of the elements was set to 25 mm. The results obtained from the simulations are almost equivalent. Only at large displacements do the load displacement curves diverge slightly. This was taken as proof that the Abaqus brittle cracking model was correctly configured, allowing its use for the simulation of the tensile splitting tests and flexural disk tests.

5.2 Size independent simulation of fracture

The most compelling reason for the use of fracture mechanics in the analysis of concrete structures is the occurrence of size-effect. In Section 4.3 it was shown that the high performance fibre reinforced concrete material is subject to significant size-effect. As a result the MOR obtained from laboratory specimens cannot be relied upon to predict the peak load for structural elements of a different size or geometry. The purpose of this section is to demonstrate that the fracture models developed in the previous section can be used to successfully predict the flexural behaviour of elements of various sizes and geometries.

5.2.1 Prediction of size effect in flexural beam tests

In Figure 5-8 a comparison is shown between the average flexural response data obtained from TPB experiments on Mix D specimens and those produced through numerical simulation. Results are plotted in terms of the LE derived nominal stress and the relative deflection of the different sizes of beams as was done earlier for the experimental results only in Figure 4-2b. The numerical simulation was performed in the OpenSees model using the softening function for mix D shown in Figure 5-5. The figure shows the model to provide a close prediction of the change in the material response for the different sizes. The use of LE based design methods would have lead to identical curves for all sizes, which is at odds with reality.

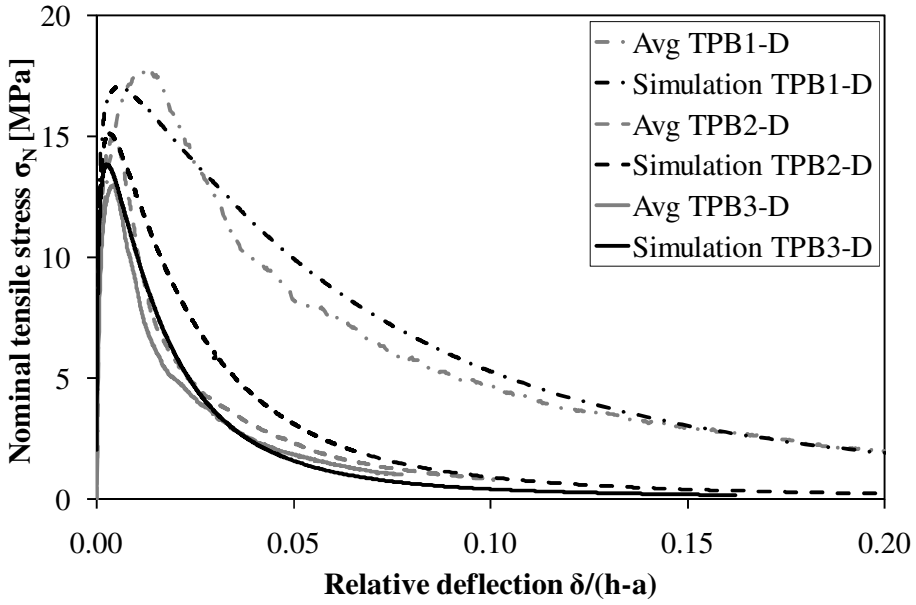

Figure 5-8: Prediction of size effect in TPB tests

The trends in the experimental and predicted σ_{Nu} size-effect for TPB and FPB specimens of mix D are shown in Figure 5-9. To show the numerical trend beyond the two FPB specimen sizes tested, the range of the modelled results was extended by simulating additional fictitious 30 mm, 50 mm and 360 mm high beams maintaining geometry. The numerical simulation provides a satisfactory prediction of the size-effect that occurred in the experiments. The experimental results do show a stronger size-effect than the numerical simulation. This is due to the fact that the numerical simulation predicts fracture mechanics size effect only. Other

sources of size-effects stemming from specimen preparation, e.g boundary layer effect, statistical size effect, hydration heat, etc. are not predicted in the numerical analysis.

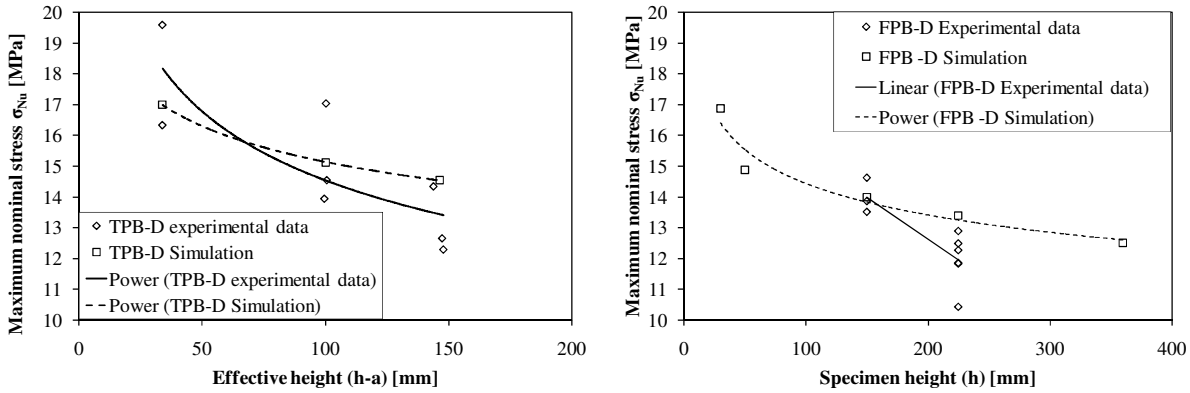

Figure 5-9: Experimental and predicted MOR size-effect trends for TPB and FPB

For the numerical simulation of specimen type TPB3-D, the stress state in the ligament above the notch at peak load is shown in Figure 5-10.

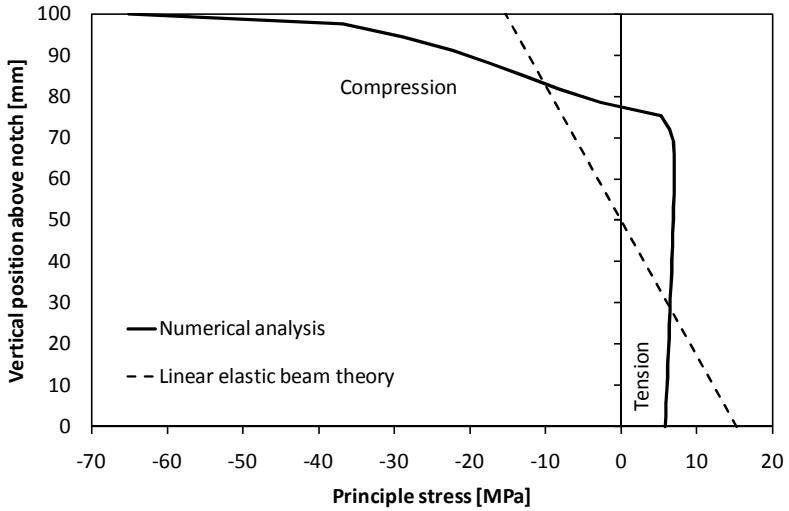

Figure 5-10: Simulated stress state at peak load for specimen TPB3-D

The fracture zone has progressed ¾ of the way up the beam. The figure provides a clear indication of the considerable difference between the proportional tension and compression

stress distribution assumed in LE analysis and the stress state in the fracture mechanics simulation. This difference in stress condition between the two approaches explains why fracture mechanics can be applied to predict the behaviour of different sized elements, while LE analysis cannot.

5.2.2 Simulation of flexural disk tests in Abaqus

The monotonic tests on disk specimens were modelled in Abaqus. A linear elastic (LE) analysis of the tests was run first to compare the results to the assumptions underlying the yield line discussed in Section 4.3.3. The second step was to analyse the disk using the cohesive crack model developed in the previous section. If the numerical simulation proofs successful, this would mean that the fracture mechanics based methodology can be used to predict the flexural behaviour of not only different sized elements, but also elements with different geometry.

In this first simulation, linear elastic material response was assumed, as would normally be done when calculating the carrying capacity of pavement slabs. The mesh for the model is shown in Figure 5-11a. Figure 5-11b shows the principal stress condition in 800 mm diameter disk at the peak load recorded in the experiments.

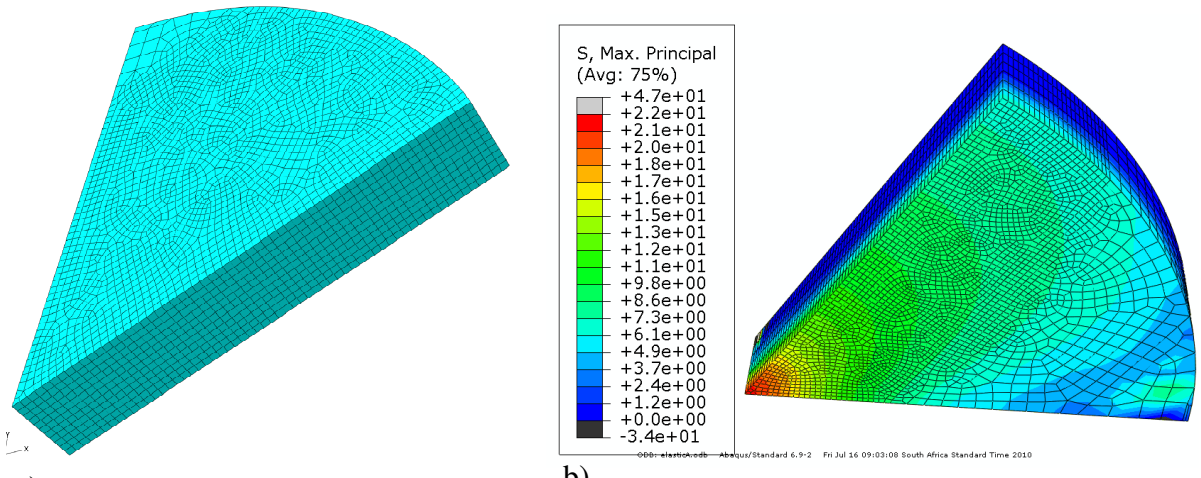

a) b)

Figure 5-11a: Mesh, b: Peak stress distribution LE model

The results indicate that the maximum tensile stresses at peak load condition are in the region of 22-24 MPa, well above MOR strength values for the material presented in Table 4-2. These peak stresses are also well above the σ_N values obtained using yield line theory as discussed in Section 4.3.3. The difference stems from the fact that in the yield line solution the stresses along the failure plane are assumed to be evenly distributed at the experimental peak load. These results indicate that if the MOR was used to predict the peak load condition of the panels, as is done in pavement design, the flexural capacity of the panels would have been underestimated. Since the MOR values for the material are between 11 and 14 MPa, the error in the prediction of the disk capacity would have ranged from approximately 70 to 100 percent.

The model can also be applied to determine whether size effect occurs in the disk test results when analysed under the assumption of linear elasticity. Figure 5-12 shows the nominal tensile stress along the symmetry line midway between two supports from the centre of the disk to the edge. In other words: along the highly stressed edge as seen on the left in Figure 5-11b. Results are shown for the 800 mm and 600 mm diameter disks prepared using Mix A and B material. The distance to the centre is plotted relative to the size of the disk. The models of the different specimen types are loaded to the respective experimental average peak load. The results show the high tensile stress at the centre of the disk. The results further indicate a slight size-effect between the results for the 800 mm and 600 mm diameter disks, with the smaller specimens providing a relatively higher loading capacity.

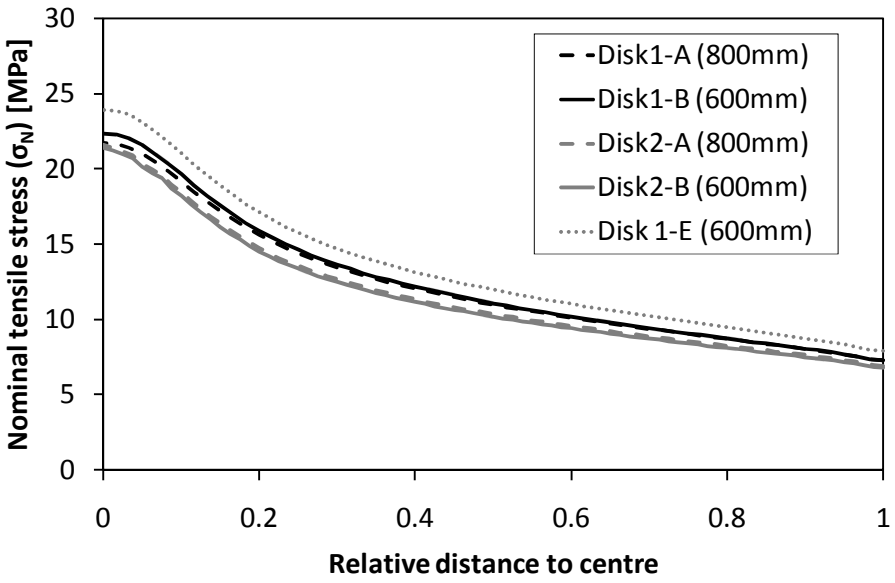

Figure 5-12: Linear elastic stress condition at mid span of disks

The next step is to numerically simulate the disk experiments using the same cohesive crack damage model applied successfully to the beams in the previous sections. The disks are modelled in using the Abaqus software environment as discussed in Chapter 3. The model and mesh for the fracture analysis are as shown in Figure 5-11b. Cohesive elements were used for the entire model, with exception of the area around the support. In this area linear elastic bulk elements were used to prevent cracks forming due to unrealistic stress concentrations.

When the initial cracks form in the model at midspan between the supports stresses redistribute leading to new highly stressed areas. Secondary cracking will occur in these areas, leading to a front of multiple cracks moving away from the main crack. This situation corresponds well to the reality of the experiments in which secondary crack patterns were observed parallel to the principal cracks as can be seen in Figure 5-13. Although the disk eventually breaks into three parts, with the failure plane approximately at the centre between the support, tension cracks have formed over a considerable area around the main cracks.

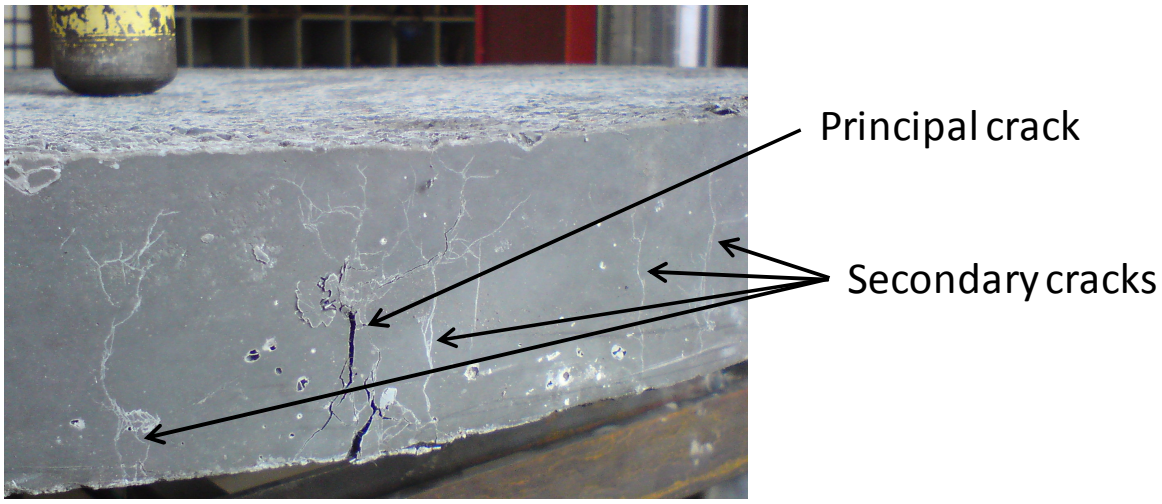

Figure 5-13: Multiple cracks forming in centrally loaded disk test

Appendix E contains the results of the numerical simulation for the different disk specimen types. Figure 5-14 shows the result of the numerical simulation for the 800 mm diameter, 70 mm high disk produced from mix A.

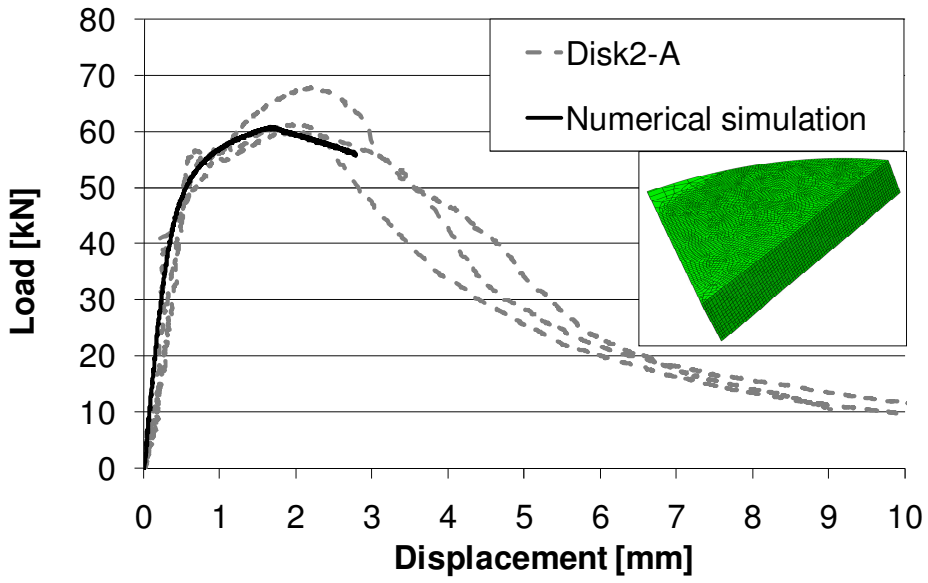

Figure 5-14: Result of numerical simulation Disk2-A

The results provide an accurate prediction of the pre-peak, peak load and early post-peak behaviour for the specimens. At larger deflections the crack tends to get locked, leading to impossibly high stresses in the material. As a result, the load carried by the slab does not decrease at the pace observed in the experiments. The simulation was stopped when crack locking started to occur. The simulation yields satisfactory results in predicting the peak load for the disks however.

The main difference between the LE and the fracture mechanics analysis is the distribution of highly stressed areas. In the LE analysis at the peak load condition recorded in the experiment, an area with unrealistic high stresses, much higher than the tensile strength or even MOR exists at the bottom around the centre of the disk. In the fracture mechanics analysis, the first cracks appear in this area when the stress reaches the tensile strength of the material. The stresses redistribute as the crack grows up and towards the edge of the slab. As the stresses redistribute, elements next to the initial cracked area start reaching the tensile strength as well and the fractured area spreads. The occurrence of additional smaller cracks, besides the three main cracks at mid span between supports, corresponds to the observations made during the experiments.

5.2.3 Summary of results for numerical simulation of unreinforced flexural tests

Table 5-1 shows the accuracy of the numerical models, in terms of the prediction of the peak load obtained in the various flexural experiments. In some cases the error is still considerable, however the prediction is far more accurate than linear elastic analysis would allow.

For some of the experiments, analysis was performed using both the exponential softening curve and the softening function that combines crack tip singularity with exponential softening. Comparing the results of the numerical simulation of beam bending tests obtained using the two softening function types however, serves limited purpose as both were calibrated against these data sets. The softening function with crack tip singularity has the following advantages over the simple exponential function:

- it resembles the documented softening behaviour of fibre reinforced concrete better,
- it allows simulation of the material behaviour observed splitting tests as will be shown in Section 5.4, and

- it allows the unaltered use of the tensile strength as obtained from tensile splitting tests as a material property.

Table 5-1: Accuracy of numerical models in prediction of monotonic peak load.

Specimen ID	P max experimental [kN]	Pmax Exponential [kN]	Error [%]	P max singularity [kN]	Error [%]
TPB1-A	41.7	39.6	4.9%	40.4	3.1%
TPB2-A	42.2	39.4	6.6%	40.5	4.0%
TPB3-A	5.6	6.7	-20.4%	6.9	-22.9%
TPB4-A	6.9	6.7	2.9%	6.9	-0.3%
FPB1-A	102.8	85.7	16.6%	91.4	11.1%
Disk1-A	39.4			39.4	0.0%
Disk2-A	63.0			60.8	3.5%
TPB1-B	43.5	40.3	7.3%	40.0	8.0%
TPB2-B	6.7	6.9	-2.6%	6.8	-1.8%
TPB3-B	7.4	6.9	7.0%	6.8	7.7%
FPB1-B	109.2	109.9	-0.6%	90.4	17.2%
Disk1-B	40.0			40.4	-1.0%
Disk2-B	61.9			61.8	0.2%
TPB1-D	12.6	11.7	7.2%	11.9	5.6%
TPB2-D	30.5	29.5	3.3%	30.4	0.3%
TPB3-D	37.4	40.7	-8.9%	41.2	-10.2%
FPB1-D	107.4	119.9	-11.6%	106.3	1.0%
FPB2-D	137.3	163.3	-18.9%	153.3	-11.7%
TPB1-E	25.5	24.7	2.9%	26.3	-3.3%
FPB1-E	101.5			101.0	0.5%
FPB2-E	49.9			47.3	5.2%
FPB3-E	12.1			12.2	-0.8%
Disk1-E	42.2			45.0	6.6%

5.3 Modelling beams with reinforcement bars

The goal of this study is to help improve the design models for concrete road pavements containing a combination of fibre reinforcement and conventional rebar. Therefore, the test matrices for Mix A and B include TPB tests on concrete beams containing reinforcement bars in addition to fibres. The effect of the rebar on the material response in TPB needs to be provided for in the numerical model for it to fully simulate material behaviour in the bending

tests. The behaviour of the steel reinforcement bars in tension has to be known in addition to the earlier discussed fracture properties of the fibre concrete mixes. A set of direct tension tests was performed on the reinforcement bars to determine elastic and plastic properties. The stress-strain relationship obtained for the rebar is shown in Figure 5-15. The average ultimate tensile strength of the bar is 550 MPa, while Young's modulus (E) was estimated at 2.11E+05 MPa from the slope of the elastic part of the curve. A typical value of 0.28 for Poisson's ratio of steel was selected. The behaviour of the rebar is modelled using the Opensees J2 Plasticity material. The element requires bulk modulus (K) and shear modulus (μ) to be defined for the elastic part of the stress strain behaviour:

$$K = \frac{E}{3(1-2\upsilon)} = 1.60\text{E}05\ \text{N/mm}^2 \tag{5.6}$$

$$\mu = \frac{E}{2(1+\upsilon)} = 8.24\text{E}04\ \text{N/mm}^2 \tag{5.7}$$

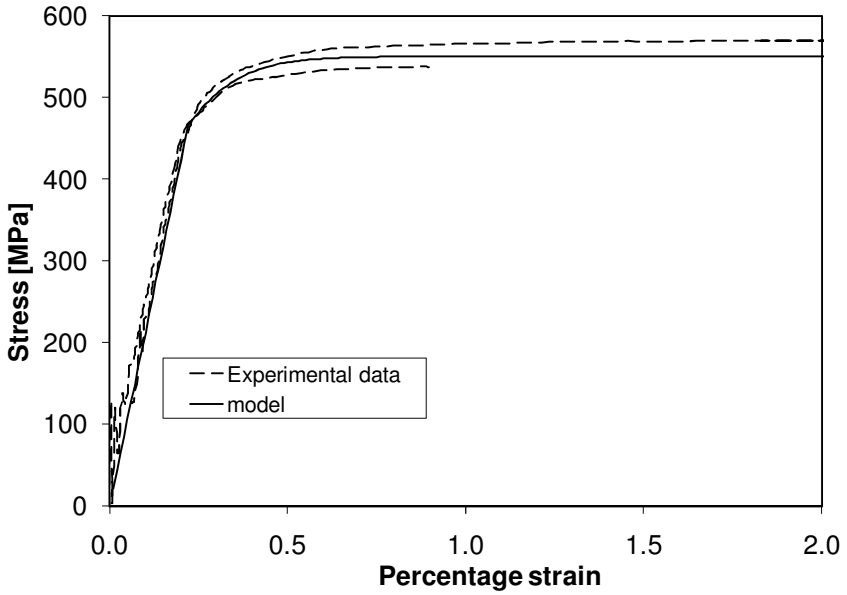

Figure 5-15: Experimental and modelled stress-strain relationship for reinforcement bars

The plastic part of the material behaviour is represented by an initial yield stress, a final yield stress level and an exponential and/or linear hardening parameter. Based on the direct tensile test results for the rebar the initial yield strength was set to 465 MPa and the saturation stress level at 550 MPa. An exponential hardening parameter of 1000 was found to provide the best fit to the test data. The result of a numerically modelled uniaxial test on the rebar with the properties described above is also shown in Figure 5-15.

The reinforcement bars are included in the numerical model as a thin strip of continuum elements. The thickness of the strip was chosen such that the cross-sectional area of the three 5.6 mm diameter reinforcement bars is divided equally over the width of the beam. Figure 5-16 shows an example comparison between the load-deflection curves obtained from the laboratory experiments and from the numerical model.

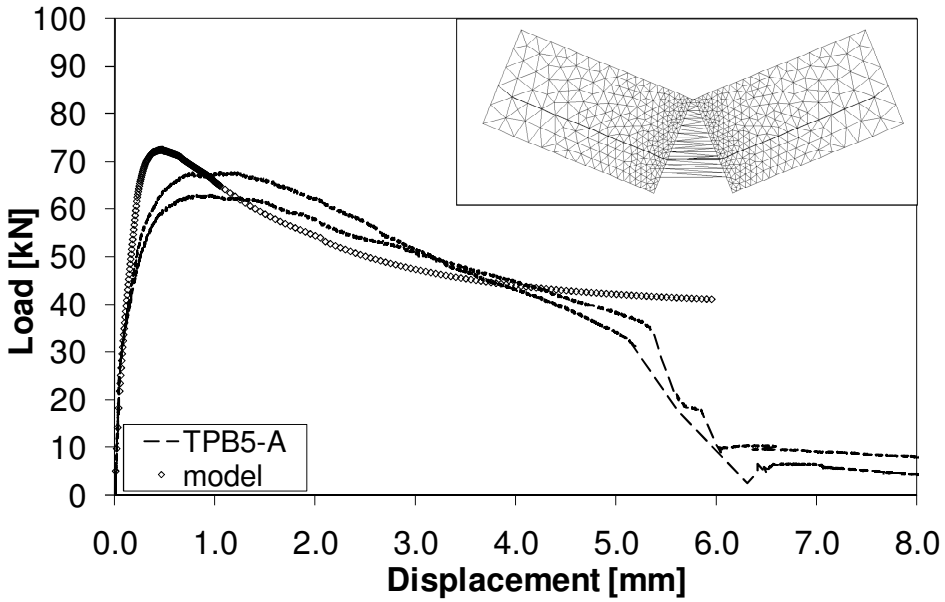

Figure 5-16: Experimental data and numerical simulation for specimen type TPB5-A including rebar

The predicted and experimentally obtained peak loads for beams of different sizes are shown in Table 5-2. The numerical model over-predicts the peak load. One of the reasons for this is the absence of bond slip; unrealistically high shear stresses are transferred to the concrete material surrounding the rebar. It would be possible to further improve the results by including a pull-out model; a number of available methods are described in Bažant and

Planas (1997). Another limitation of the current model is that the eventual tensile failure of the reinforcement bars cannot be covered by the J2 Plasticity material. Therefore, the model does not show the sudden drop in load level that can be identified in the experimental data in Figure 5-16 at approximately 5.5 mm deflection. Notwithstanding these two limitations the model was found to provide a satisfactory prediction of the peak load and the shape of the load-deflection curve. Importantly, this exercise shows that it would be possible to include rebar in the fracture mechanics analysis of concrete pavement structure.

Table 5-2: Comparison between predicted and actual peak loads for beams with rebar

Specimen type (Mix A + 3Y5.6)	**TPB5-A**	**TPB6-A**	**TPB7-A**	**TPB8-A**	**FPB2-A**
P_{max} [kN] Experiment	65.4	64.1	10.5	11.6	116.5
P_{max} [kN] Simulation (G_f = 5.0 N/mm, f_t = 5.8 MPa)	72.3	73.1	13.9	14.0	159.9
Percentage error [%]	10.6%	14.0%	32.4%	20.7%	37.3%
Specimen type (Mix B + 3Y5.6)		**TPB4-B**	**TPB5-B**	**TPB6-B**	**FPB2-B**
P_{max} [kN] Experiment	-	64.4	12.6	13.4	141.2
P_{max} [kN] Simulation (G_f = 5.5 N/mm, f_t = 5.9 MPa)	-	75.6	14.1	14.1	161.3
Percentage error [%]	-	17.4%	11.9%	5.2%	14.2%

5.4 Numerical model of tensile splitting test

The adjusted tensile splitting experiments were simulated using the Abaqus model discussed in Section 3.3.2. The simulated load-transversal deformation response for the different mixes is shown in Figure 5-17. The simulation is successful in predicting the first peak load P_I at which a crack is introduced. If the obtained P_I values are used to back-calculate f_t using Equation 4.19 the results are within 1 percent of the input value. This confirms the need to use the correction for boundary conditions proposed by Tang (1994), on which Equation 4.19 is based. Importantly, the results of the numerical simulation shows a similar trend to the experimental results, after reaching the first peak, the load level stabilizes and then starts to increase again. This phenomenon is caused by the use of the softening function with crack tip singularity.

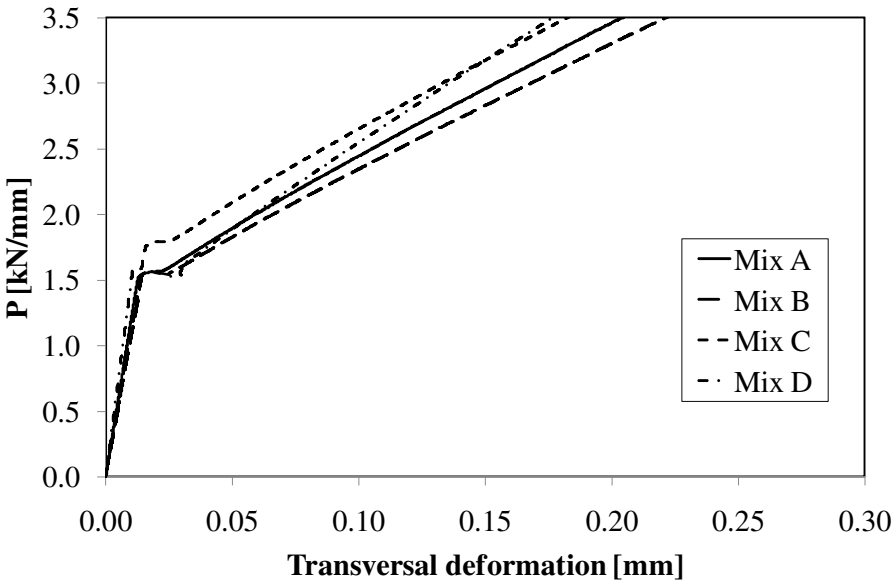

Figure 5-17: Simulated load-transversal deformation response

The numerical analysis allows a study of the stress distribution at the different stages of the test. Figure 5-18a shows the principal stress distribution just before a crack forms at the centre of the specimen. This is the linear elastic stress distribution assumed when calculating the tensile strength from the splitting test using Equation 4.19.

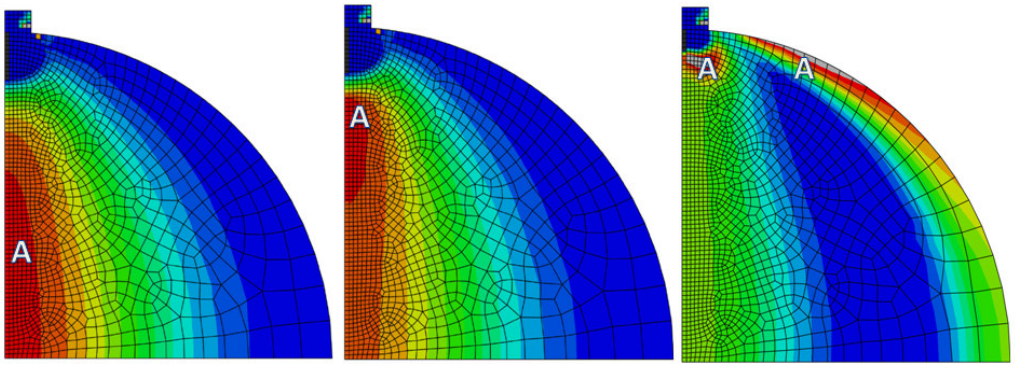

a) b) c)

Figure 5-18: Principal stress distribution in numerical model of splitting test

Highly stressed areas are indicated in the figure with “A”. Once the tensile strength is reached, a crack forms at the centre of the specimen and propagates upward as shown in

Figure 5-18b. The stress redistribution following the initial peak load, shown in Figure 5-18c, sees the relaxation of stresses along the loading axis and the formation of highly stressed areas at the top and the side of the specimen. The stresses in these areas exceed the tensile strength of the material and would lead to secondary cracking as discussed in Section 3.2.6. The model however does not contain fracture elements in these regions and therefore no secondary cracking occurs in the simulation. Consequently, the load- transversal deformation curves in Figure 5-17 do not yield an ultimate load P_u value.

The numerical simulation of the tensile splitting tests confirms that the ultimate peak load is related to secondary cracking mechanisms. The first peak P_I represents the linear elastic limit state and from it a best estimate of the tensile strength material property can be calculated.

5.5 Application of the damage model to simplified pavement structure

The numerical simulation and analysis in this document have so far been confined to laboratory experiments. To further explore the use of fracture mechanics in pavement design, a simple hypothetical pavement structure is analysed. The numerical analysis is run using LE and fracture mechanics material behaviour for the concrete pavement slab. Figure 5-19a shows the boundary conditions of a simplified pavement system. A 50 mm thick slab was modelled using the material properties of Mix E. The slab is supported by a 950 mm thick base with a E value of 200 MPa, on a stiff support. The load case is a classical corner load on the free edge of the slab. The area of the structure is 1.8m x 1.8m, with symmetry boundary conditions on two of the edges of the slab, making the effective size of the model 3.6 m x 3.6 m. The pressure loading is applied on a 100 mm x 100 mm patch using a ramp function. The mesh for the pavement slab consists of two layers of elements with a characteristic size of 25 mm. The elements for the elastic base layer are larger. The model is simplistic and not representative of an in situ pavement, UTCRCP or other, nor is the meshing optimal for analysis of a pavement. This simple model is however deemed suitable to compare the behaviour of a pavement slab with LE material properties and a slab with a cohesive crack damage definition on an elastic support.

Figure 5-19b and Figure 5-19c show a comparison between the results obtained for the simulation of stresses in a slab consisting of LE and for a slab consisting of elements with cohesive fracture damage definition. The pressure load on the LE model was increased until

the tensile stresses in the slab were equal to the MOR value of 13.9 MPa as obtained for the material from FPB tests on beams with a 150 mm x 150 mm cross section (refer Table 4-2). This occurred at a pressure of 3.36 MPa in the loaded area, equal to an external load of 33.6 kN. Coincidentally, this is representative for the load applied by the wheel of a truck steering axle. The resulting stress distribution in the pavement is shown in Figure 5-19b. The stress distribution in the slab with the cohesive crack damage definition under the same loading is shown in Figure 5-19c.

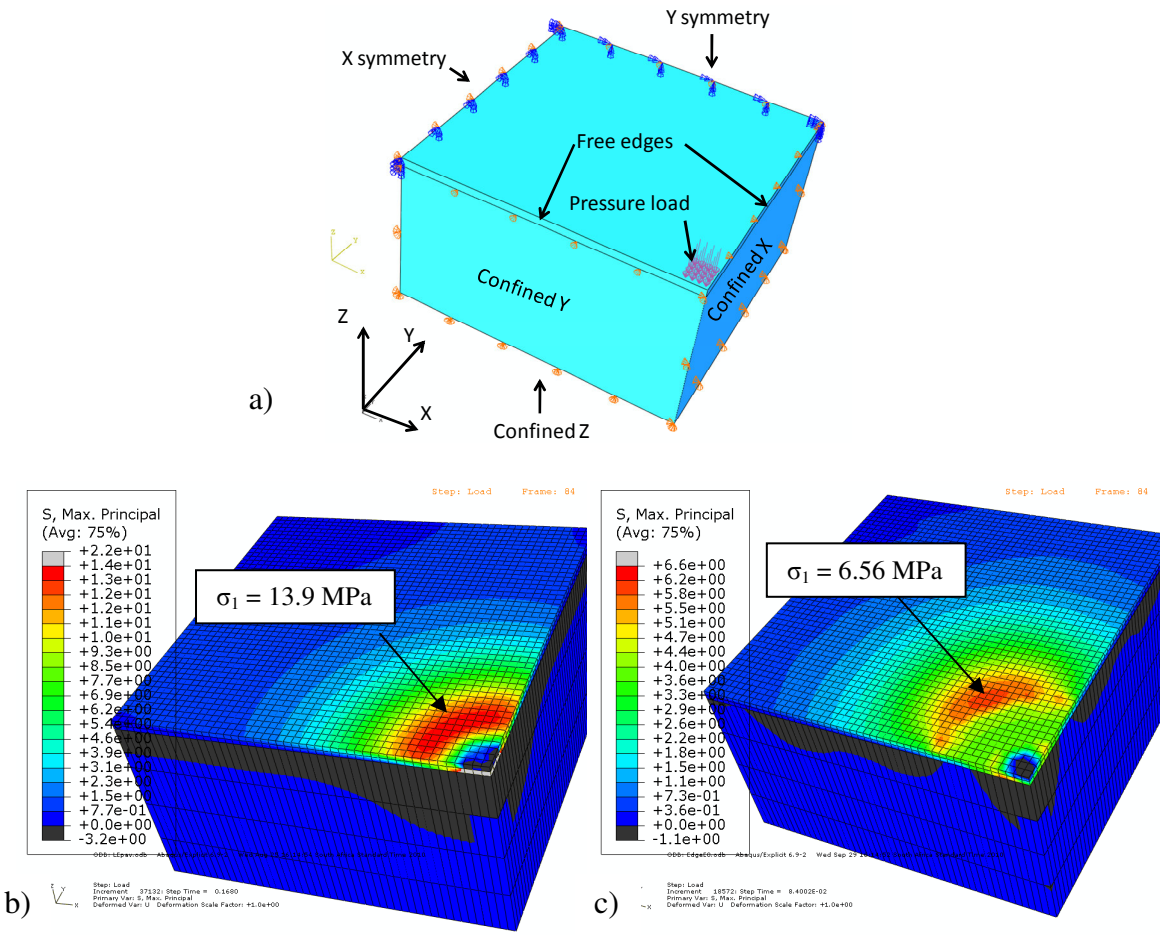

Figure 5-19a: Boundary conditions FRC pavement model, b: Result LE analysis, c: Result fracture model.

Fracture occurs at a tensile stress of 6.56 MPa, the first crack formed in the same area where the highest tensile stress occurs in Figure 5-19b. Further loading results in the cracks forming in elements further away from the slab edge. At the final 33.6 kN load condition, the stress area for which the highest stress occurs in the LE analysis has decreased significantly due to softening in the crack model. The main implication is that at stresses of approximately 50 % of the MOR cracks are introduced to the pavement causing stress relaxation. The comparison

shows that LE analysis leads to unrealistically high stresses that cannot occur in the material. As discussed in Chapter 2, fatigue performance of the pavement is predicted in conventional theory by the ratio of the LE derived stresses in the pavement slab to the MOR of the material. The purpose of this example is to show that the fatigue function is based on an unrealistic analysis of the stresses in the pavement slab.

A third analysis was run to investigate the load needed to completely break the slab under monotonic loading. Figure 5-20a shows the load displacement curve for the fracture mechanics based concrete pavement model. The slope of the load increase will be greatly dependent on the stiffness of the subgrade. The pavement slab fails at a load of approximately 85 kN and a deflection of 10 mm. This can be observed by the change in slope of the graph in Figure 5-20a at 10 mm deflection. The major principal stress condition in the pavement at time of failure of the slab is shown in Figure 5-20b. The principle stresses have dropped below the maximum tensile stress of 6.56 MPa over the entire area. The displacements have been scaled five times in the figure to enhance visibility. This type of analysis may provide a suitable point of departure for fatigue prediction, as it provides an indication of peak load capacity at failure similar to what is recorded in beam bending tests and disk tests.

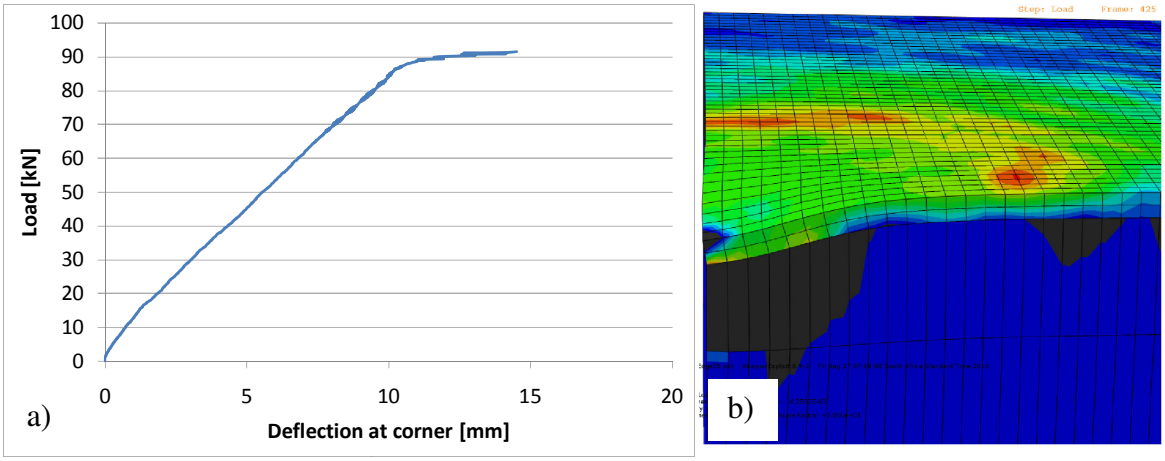

Figure 5-20a: Load-displacement curve for pavement structure, b: Major principal stress condition at failure concrete pavement (displacement scale x5)

For comparative purposes, a similar analysis was run for a plain concrete pavement. The material properties were based on the test results from phase 2 and the softening function developed for this 40 MPa plain concrete material tested at UC Davis. The model is shown in Figure 5-21a. The boundary conditions are the same as for the FRC pavement, but the slab

thickness was increased to 200 mm, which is more representative for plain concrete pavements. The results of the LE analysis of the concrete slab are shown in Figure 5-21b, the results of the fracture mechanics based analysis are shown in Figure 5-21c. As before, a pressure load was applied to the LE model until the principal stresses in the slab reached the nominal maximum stress value of 4.7 MPa determined in the flexural beam experiments. This occurred at a pressure loading of 6.5 MPa on the loading patch, which corresponds to a 65 kN total load. The same pressure load was then applied to the fracture mechanics model. This example again shows the difference in the stress condition calculated using LE analysis and the more advanced fracture mechanics based model. It is proposed that the fracture mechanics model provides a more accurate picture of the stress condition in the pavement and the location of progressive (fatigue) damage formation.

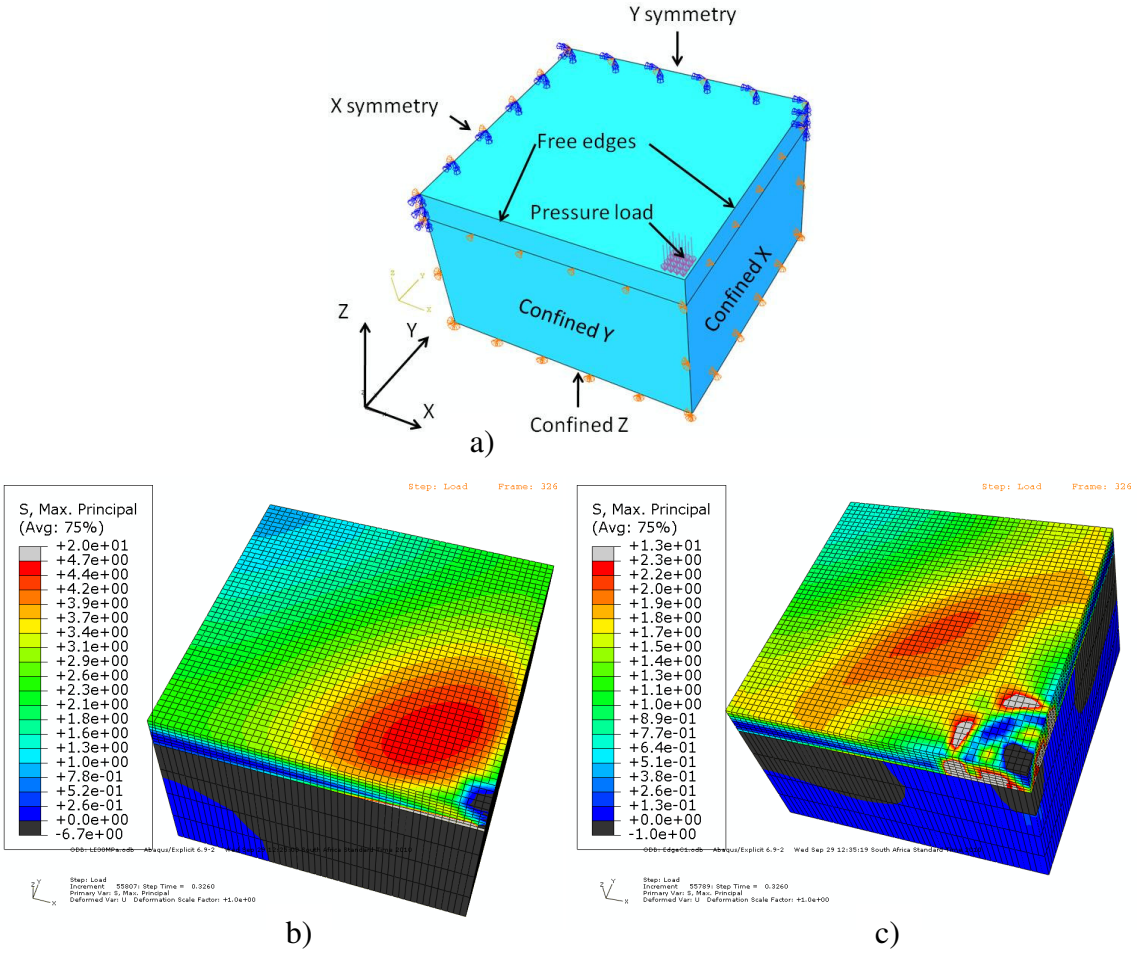

Figure 5-21a: Boundary conditions plain concrete pavement model, b: Result LE analysis, c: Result fracture model.

5.6 Fatigue fracture prediction

In the previous sections it was shown that fracture mechanics concepts can provide a more accurate prediction of the flexural behaviour of high performance fibre reinforced concrete under monotonic loading. The next step is to assess whether fracture mechanics principles can be applied to increase the accuracy and precision of fatigue prediction models. To this aim, a model for the prediction of fatigue is calibrated using the approach applied in conventional pavement design methods. Once this model is defined, alternative models based on fracture mechanics approached are calibrated, to explore whether more precise predictions can be obtained. The fatigue tests on the FPB specimens with 150x150mm^2 cross section are used as the benchmark for calibration. The models are then compared in terms of their predictive performance for the fatigue life recorded in experiments on specimens of different sizes and geometry.

5.6.1 Fatigue prediction using the conventional method

In conventional pavement design, the fatigue life is calculated based on the ratio of the maximum tensile stress (σ_d) in the concrete slab calculated using LE analysis of the pavement structure and the MOR, i.e. the maximum nominal tensile stress (σ_{Nu}) achieved in standardized FPB tests. The form of the fatigue model as used in the current South African concrete pavement design, shown earlier as Equation 2.3, is maintained here:

$$N = a_1\left(\frac{\sigma_d}{MOR}\right)^{b_1} \tag{5.8}$$

The test results for the 150 mm x 150 mm cross section FPBF1-E are shown in Figure 5-22. The power function shown in Equation 5.8 is fitted to the results. The best fit with an R^2 of 0.79 is obtained for a_1 = 2526 and b_1 = 14.21. In the figure the power curve is extrapolated to show the prediction of the model at different stress levels.

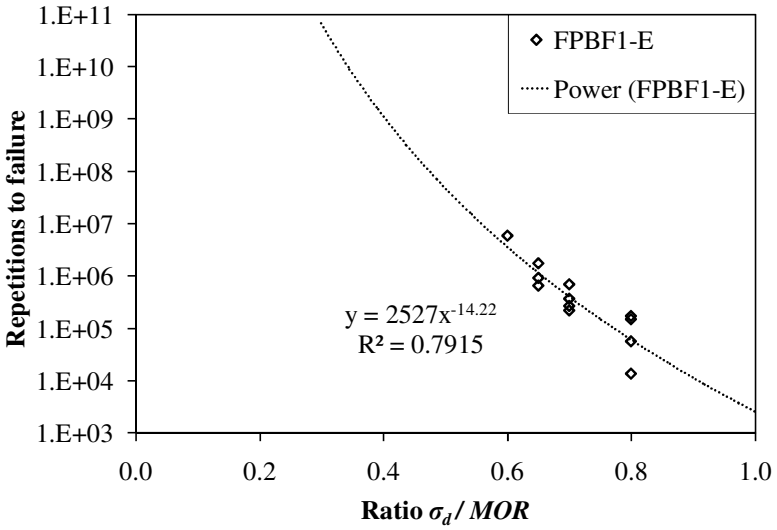

Figure 5-22: Calibration of conventional fatigue model

An interesting point to note here is that many concrete pavement design methods, including the current South African method and the new American method according to NCHRP 1-37 use a power shape to represent the performance of concrete at different stress levels. This in contrast to the logarithmic function that is typically fitted to the data in fatigue studies on concrete, e.g. Lee and Bar (2002). The choice of the shape of the curve is important, because pavement design typically concerns large numbers of load repetitions to failure. This will often involve extrapolating the model beyond the range of experimental fatigue data against which it was calibrated. Such extrapolation will yield significantly different results for power function curves than for logarithmic functions.

The predictive performance of the conventional fatigue model for specimens of different sizes and geometry is Figure 5-23. The vertical axis shows the ratio between the peak stress (σ_d) in the different specimens calculated using LE theory and the peak stress σ_{Nu}. (MOR) from FPB tests on 150 mm x150 mm cross section.

The model performs relatively well in predicting the fatigue life of the 100 mm x 100 mm and 50 mm x 50 mm beam specimens the relationships for which are shown in Figure 5-23a and Figure 5-23b. Note that due to size effect, these specimens failed at a higher peak stress than the 150 mm x 150 mm specimens and since the tests were performed at fixed percentages of the peak load for each beam size, the specimens were therefore tested at a higher stress level compared to the 150 mm x 150 mm specimens.

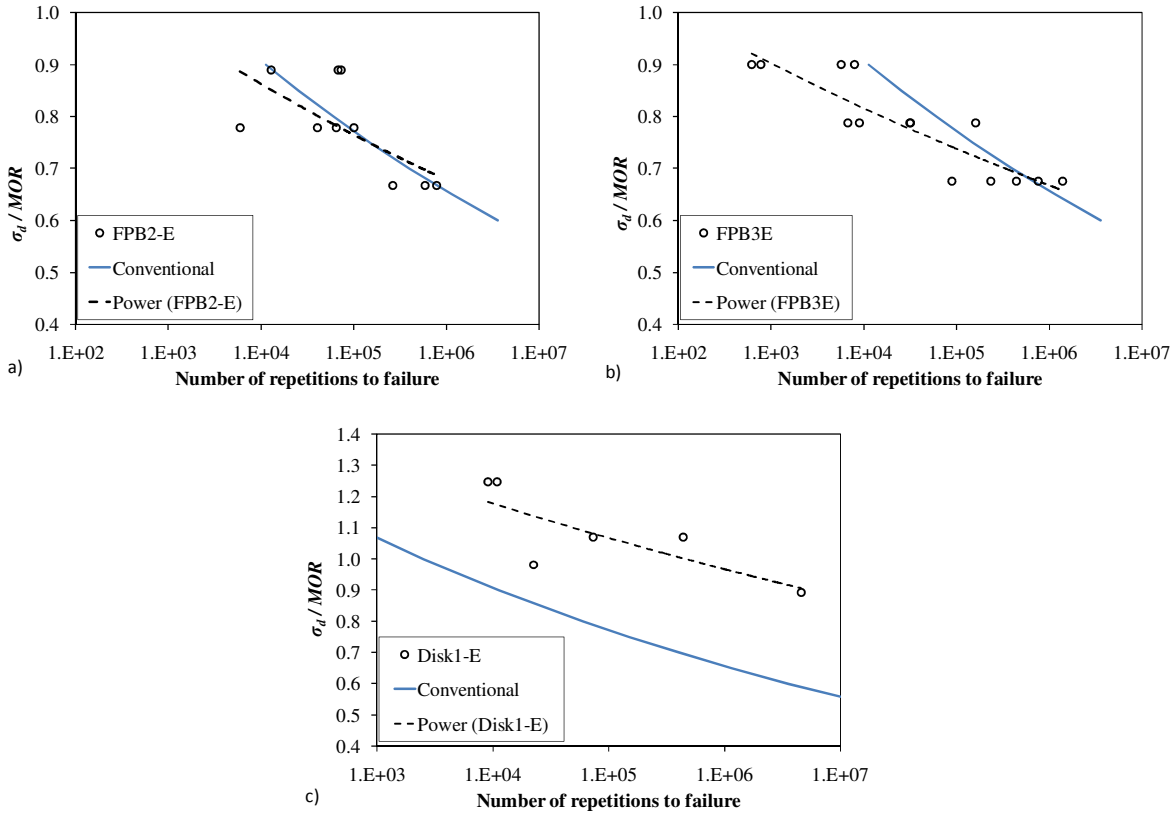

Figure 5-23: Predictive performance of conventional fatigue model for: a) 100 mm high beams, b) 50 mm high beams and c) 600 mm diameter disk specimens

There is some indication from the relative trajectory of the power functions, that at lower stress levels, the model may start to under-predict the fatigue life. The performance of the model for the prediction of the fatigue life of the disk specimen as shown in Figure 5-23c is less than satisfactory. The predicted number of load repetitions to is 100 times smaller than the actual number of load repetitions to failure. The limitations of the MOR as material property combined with LE analysis of the disk become visible here. The disk tests were performed at load levels, which according to LE analysis results in stresses higher than the MOR of the material.

For the calibrated functions used in pavement design the gap between the results predicted by LE theory and the results obtained from large scale experiments or data from actual pavement structures would have been remedied by the use of shift factors. In other words, statistical calibration of Equation 5.8 to fit data from the field, without mechanistically addressing the limitations of LE analysis.

5.6.2 Fracture mechanics based method

For the development of a fracture mechanics based model a number of observations and findings made previously in this study can be used:

- The cohesive crack model developed in the study can be applied to reliably predict the behaviour of the UTCRCP material in monotonic flexure,
- The cohesive crack model can probably also be used to calculate the crack length at different levels of displacement,
- It may be assumed that the stress at the crack tip will be equal to the tensile strength of the material determined from the tensile splitting test.
- The load-displacement envelope of monotonic experiments or monotonic loading fracture mechanics analysis of a structure may provide a good indication of the displacement at failure in the fatigue tests,
- The fatigue tests indicate that the equivalent energy (G_E) dissipated at the time of failure may be constant and independent of specimen geometry for fatigue tests on a material.

The challenge is to find a reliable model for the prediction of fatigue that is practical enough to be used and calibrated for general application in pavement engineering.

5.6.3 Peak load based fatigue prediction model

The point of departure for the development of a first fracture mechanics based fatigue model is that the main limitation to the current fatigue predictions may not lie in the statistical calibration to fatigue data, but instead lie in the simple LE analysis of the stresses in structural elements. The first attempt to develop an improved fatigue model is therefore based on the improved understanding of the stress state in the specimens allowed by fracture mechanics analysis.

Both stress parameters in Equation 5.8 suffer from the assumption that the material behaves linear elastically. As a result, the value of the stress (σ_d) calculated for a pavement structure will be unrealistic in case its value is higher than the tensile strength (f_t) of the material. The other parameter, the MOR is subject to size effect, again as a result of the LE assumption. In reality cracks form well before the peak load in the FPB test is reached and the stress therefore never reaches the MOR value.

An improved model can be devised that draws on the fracture mechanics models developed in this study by simply replacing the LE derived stress parameters in Equation 5.8 by values calculated using fracture mechanics. The use of the stress condition would be complex, because according to the model, once f_t is reached, the stress becomes a function of the crack width, with the possibility of multiple cracks forming in the structural element. Therefore, instead of the stress, the load applied to the element is used. The equation becomes:

$$N = a_1 \left(\frac{P_d}{P_{du}} \right)^{b_1} \tag{5.9}$$

Where P_d is the load total of external loads applied to the element, and P_{du} is the peak load for the element derived through numerical simulation using a fracture mechanics approach.

The model is again calibrated against the fatigue results for the 150 mm x 150 mm cross section FPBF1-E specimens. This of course results in exactly the same fit, as the MOR is the LE stress condition calculated from the P_{du} value on these specimens.

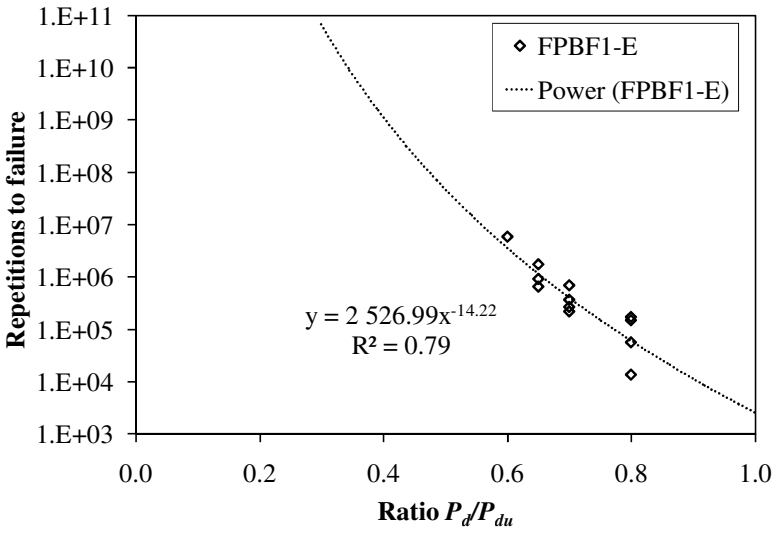

Figure 5-24: Calibration of fracture mechanics based fatigue model

The predictive performance of the fracture mechanics based fatigue model for specimens of different sizes and geometry is shown in Figure 5-25. The figure shows the results based on the value of P_{du} calculated using the cohesive crack model developed in the previous chapter. The cohesive crack model has a high accuracy in the prediction of the peak load however,

there will always be a certain error as was shown in Table 5-2. For comparison purposes the results for the fatigue model are also shown for the optimum situation where there is a 0% error in the prediction of the average peak load from the numerical simulation.

Compared to the results of the conventional model, the prediction of the fatigue life of the 50 mm x 50 mm specimens in Figure 5-25a and of the 100 mm x 100 mm specimens in Figure 5-25b, using the fracture mechanics based approach is less accurate. This is a consequence of the size effect predicted in the numerical simulation, which is not visible in the fatigue test results. As shown in Figure 5-25c, the fracture mechanics based model provides a slightly more precise prediction of the fatigue performance of the disk. The error however is still significant. The predicted fatigue values are about 30 times larger than the actual values. The predictive performance of the equation for specimens of a different geometry is not as encouraging as expected.

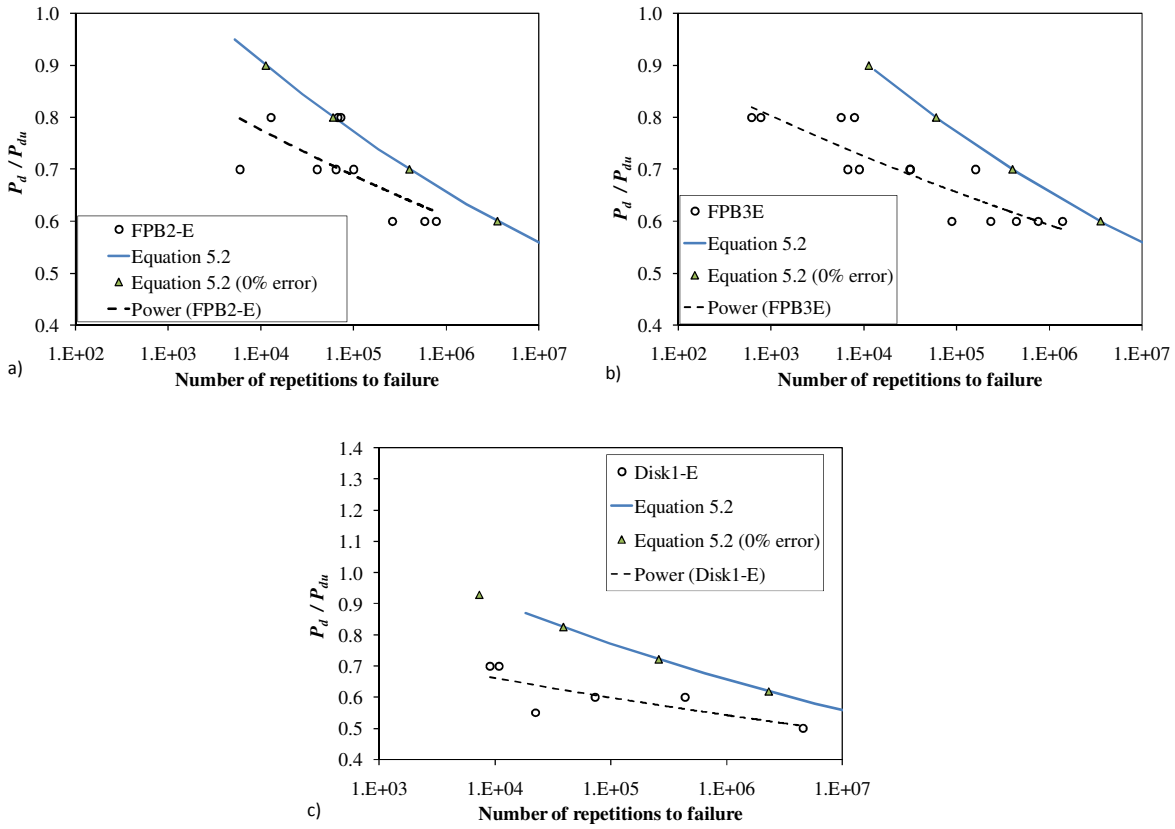

Figure 5-25: Predictive performance of fracture mechanics fatigue model for: a) 100 mm high beams, b) 50 mm high beams and c) 600 mm diameter disk specimens

To apply the predictive fatigue to a full size pavement structure, it would be necessary to separate the load absorbed by the pavement structure from the load absorbed by the slab. The loading required to break the slab representing P_{ud} for the fatigue model. This may be possible by loading the pavement slab to complete failure in the numerical simulation as shown Figure 5-20a and then unloading the structure to obtain the elastic response offered by the substructure.

5.6.4 Deflection based fatigue prediction model

Previous studies have shown that, although the monotonic load-displacement curve is not valid as an envelope for load-displacement response under cyclic loading, it may be applied as such to fibre reinforced concrete. The data from this study seems to support the theory that failure occurs in cyclic testing when the deflection approaches the monotonic envelope.

The next attempt to model fatigue is therefore based on the relationship between the displacement at the peak of the initial load cycle (δ_0) and the displacement at the peak of the final cycle before failure (δ_1). In Figure 5-26, the model is shown schematically for the simulated load-displacement curve for the FPB1-E test. The positions of δ_0 and δ_1 are shown for the case where the cyclic loading is performed at 60 percent of the peak load. The assumption in the model is that the monotonic curve as obtained from fracture mechanics analysis acts as envelope for the displacement in the fatigue tests. Note that this model is equivalent to a model based on comparing the work of fracture applied in the first cycle to the work of fracture dissipated at the last cycle.

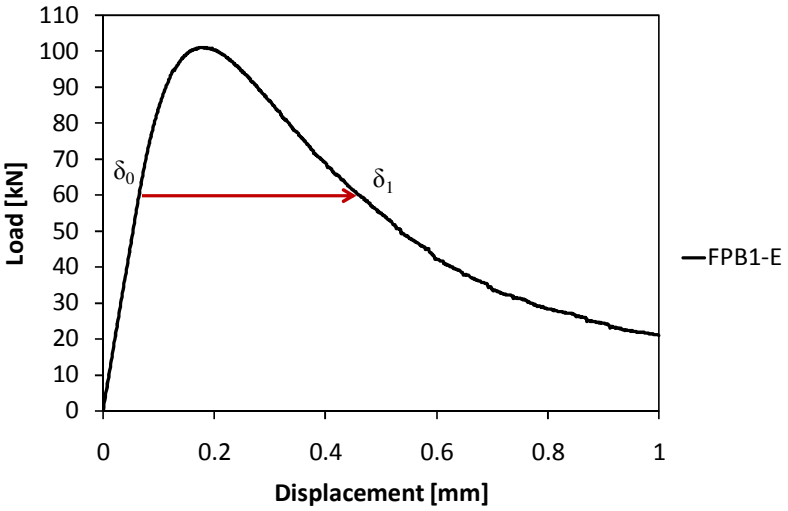

Figure 5-26: Displacement based model

Once again, the familiar power function is calibrated. The displacements at the different load levels are obtained from the load-displacement curves from the numerical simulation of the various specimen types. The fatigue model based on the displacement ratio is shown below. The power function fit to the data for the 150 mm x 150 mm beams is shown in Figure 5-27. Values of 1.098 and -5.1 were found for parameter a_1 and b_1 respectively.

$$N = a_1\left(\frac{\delta_0}{\delta_1}\right)^{b_1} \tag{5.10}$$

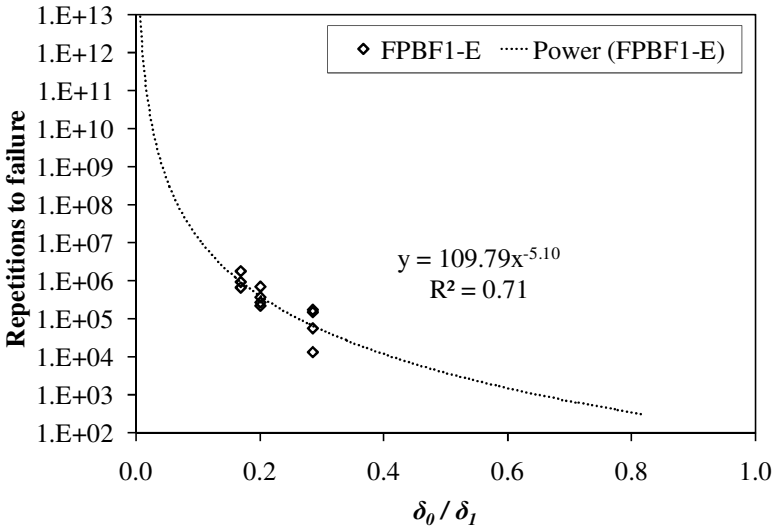

Figure 5-27: Calibration of displacement based fatigue model

Unfortunately, the model shows severe limitations in the prediction of the fatigue life for the 100 mm and 50 mm high beams as well as for the disks as shown in Figure 5-28. The lack of fit may be caused by the difference between the predicted load-displacement envelope and the actual displacement at which failure under cyclic loading occurs. The lack of fit may also indicate that there is little correlation between the relative horizontal distance between δ_0 and δ_1, and the fatigue life. This is opposite to what was expected however, as δ_0 and $\delta 1$ are indicators of W_{ff} and the dissipated energy G_E, which were found to be consistent. The prediction of fatigue based on the dissipated energy or deflection may require a different approach.

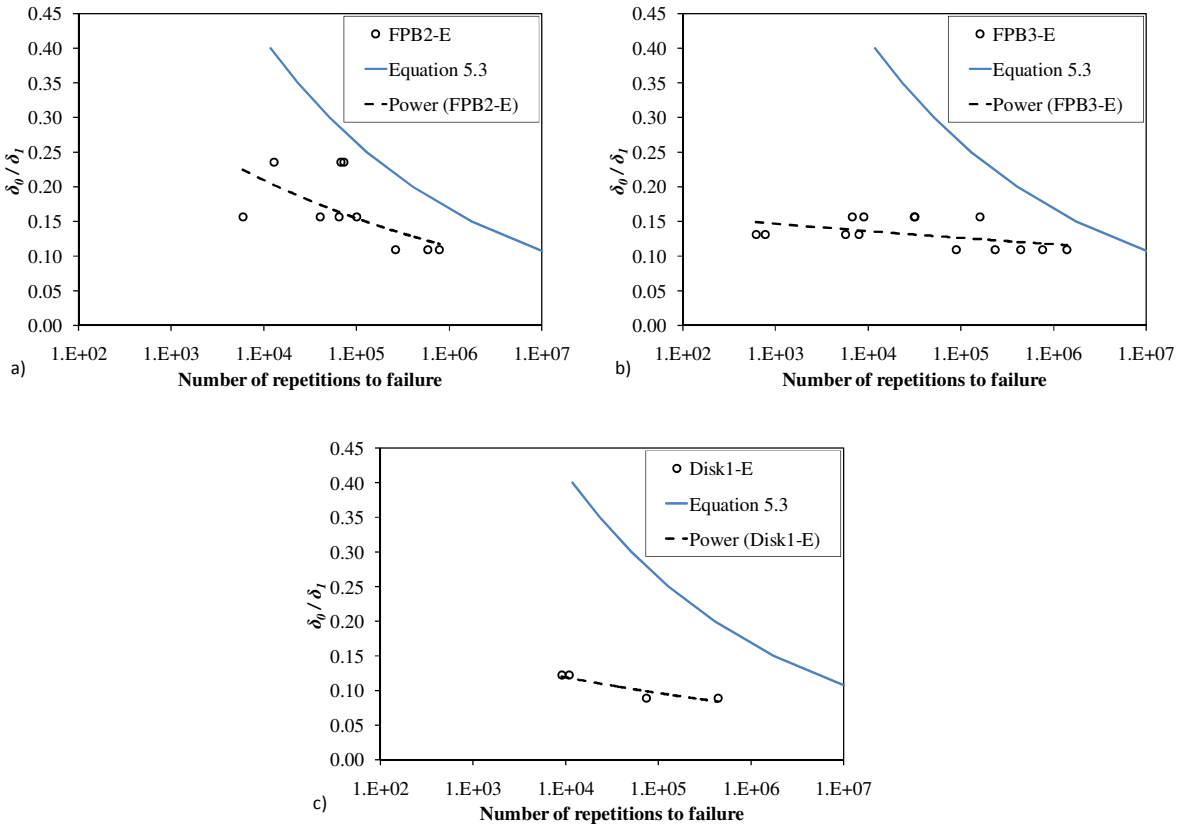

Figure 5-28: Predictive performance of displacement based fatigue model for: a) 100 mm high beams, b) 50 mm high beams and c) 600 mm diameter disk specimens

5.6.5 Model based on crack length

As discussed in Chapter 2, researchers have previously developed methods based on Paris' equation to predict fatigue fracture propagation. For such models data on the increase in crack length per load cycle is required. This data could be compared to the increase in crack length in monotonic tests. It is possible using the numerical simulation models presented in this document to track the effective crack length a in the specimens under increasing monotonic load. Figure 5-29 shows for the different specimen sizes, the crack length (a) relative to the specimen height (h), plotted against the ratio of the applied load (P) and the peak load (P_u).

The effective crack length under cyclic loading can be derived from the load compliance and effective stiffness recorded in cyclic experiments. The measuring equipment and sample rate used in the cyclic experiments in this study however, are not suitable to calculate a precise estimate of the effective crack length development. A predictive model for fatigue behaviour

based on the effective crack length from monotonic tests will only yields a similar result as the model based on deflection unless it can be calibrated against actual crack length data from cyclic tests. The development of a fatigue model based on crack length is therefore not pursued any further as part of this study.

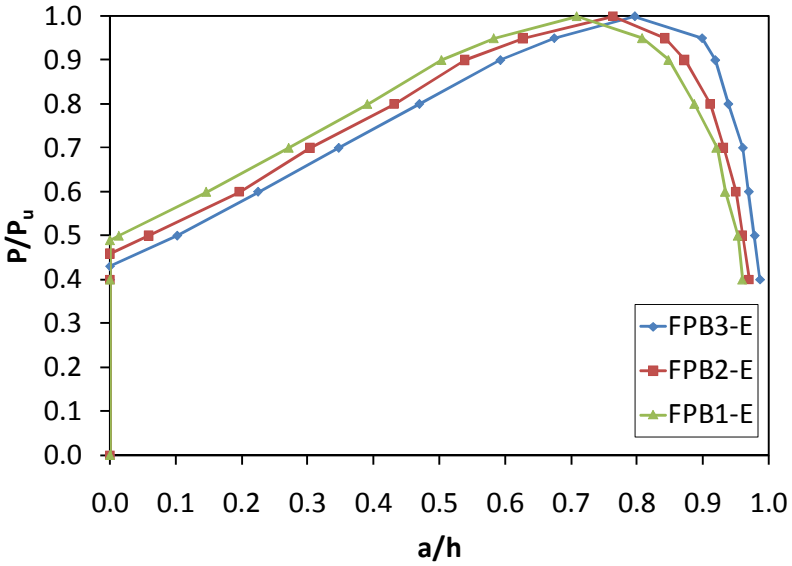

Figure 5-29: Fracture propagation in beams of different sizes.

5.7 Discussion on the numerical simulation of fracture

In this chapter, the fracture properties G_f and f_t determined for the various materials in the previous chapter, were used to define a cohesive crack softening function. The initial simple exponential softening function was completely defined using only the two parameters G_f and f_t. Exponential softening provided satisfactory results for the analysis of fracture in the plain concrete specimens, but it did lead to over-prediction of the peak load for the FRC specimens.

A shape that better suites the softening behaviour of fibre reinforced concrete was constructed by combining crack tip singularity with an exponentially softening tail. It was shown that this model allows for the reliable prediction of the opening mode fracture behaviour of the high performance fibre reinforced concrete material. The shape of the softening function is defined by four parameters, i.e.: Gf, f_t, a standard crack opening width at

which the fibres are activated w_1 and a third parameter σ_1 representing the crack bridging stress at the base of the singularity, which is obtained through calibration. The ability of the method to simulate the fracture behaviour of specimens of different sizes and geometry shows that the calibration of σ_1 is justified.

In essence, it is possible to use the fracture properties obtained from flexural beam experiments and numerically predict the structural capacity of specimens of a different size, different geometry and/or different loading conditions such as the splitting test. The test configuration developed in the chapter, together with the numerical models presented, can be applied with confidence to predict the flexural and tensile capacity of UTCRCP material. This in contrast to the MOR parameter, which because of size effect cannot be used to make reliable predictions.

It was shown in this chapter that the size-effect can to a large extent be predicted through the use of fracture mechanics. The models also provide insight in the cause of size effect, showing that cracks start propagating well before the peak load in a flexural beam test is reached. This clearly shows the error in the assumption that a linear elastic stress distribution exists at the peak load condition in the MOR test. The limitations to LE analysis of structures produced from the high performance fibre reinforced material were also highlighted. If LE analysis combined with the MOR obtained from beams had been used to predict the peak load of the flexural tests on the centrally loaded disk specimens, this would have lead to an underestimation of the capacity of approximately 100%. The analysis of the simplified pavement system showed the LE analysis may result in unrealistic stress conditions. In conventional pavement design, the stresses calculated in this manner are used in the stress/strength ratio for the prediction of fatigue life. The cohesive crack model on the other hand can be used to obtain a more realistic estimate of the stress condition in the pavement.

The precision of the results of the numerical simulation indicate that the methodologies to obtain the specific fracture energy through extrapolation of the TPB load displacement tail and the tensile strength from the adjusted tensile splitting test are fit-for-purpose.

The developed methods could be used for application beyond the scope of the present study. The model with the cohesive crack damage definition could, for instance, be used to predict the crack patterns in the pavement slab by loading the model with a moving load, or simply by putting loads in different positions on the slab. The models may also be used in the design of FRC structural elements for application outside the field of pavement engineering.

At present the fatigue prediction models developed in this chapter are based on the experimental results obtained for a single mix. A laboratory test programme is currently underway which comprises a similar test matrix as used for Mix E, applied to a mix with 80 kg/m^3 fibres and one without fibres. The results of these tests will allow the further development and/or generalization of the models presented here.

Two models were developed, one based on the peak load of the structural element obtained through fracture mechanics analysis, the second based on the deflection of the element as predicted through fracture mechanics analysis. A third model based on the prediction of equivalent crack growth was not pursued further than an initial investigation, due to a lack of suitable data.

The model based on the fracture mechanics derived peak load shows some promise. It could be argued that the precision of the prediction was still poor even though it outperformed the conventional approach. However, in light of the broader findings of this study it is proposed that the model is based on a more accurate description of the fracture mechanism at play. It provides a practical method to relate the improved understanding of crack formation in the material allowed by fracture mechanics to the prediction of fatigue performance. It could be applied to a full size pavement simply by implementing the cohesive softening model for the concrete slab and analysing the response of the system to a static load. It is argued that although the model is not perfect (no model is), it is an improvement to the conventional approach. The model however still relies on statistical calibration for the prediction of fatigue fracture propagation. The mechanism of damage evolution, the gradual tensile softening of the material with the increase in load cycles is not addressed by the method. In essence, the fracture performance of the material in fatigue is related to the fracture performance of the material under monotonic loading through simple calibrated power function.

The model was calibrated using a power function mainly because conventional design methods use this shape. The power function however, results in a very high number of repetitions to failure at low load levels compared to logarithmic functions. This study did not produce data to validate the fatigue performance of the material at low stress levels. In general, due to the practical difficulties in running tests to more than 10^7 cycles, there is little or no data available for fatigue performance of concrete below 50% of monotonic peak load. The results of this study and the literature consulted as part of this study, do not necessarily support the choice for a power function over a logarithmic function. This observation is made

here merely to indicate that in pavement design fatigue is predicted for high cycle applications. Typically the number of load applications carried by a pavement will be at the high end if not beyond the range of the available fatigue data from laboratory experiments. Extrapolation of the available data makes the choice between a power function, or an exponential function an important one.